



ORIGINAL ARTICLE

Simultaneous determination of Hg(II) and Cu(II) in water samples using fluorescence quenching sensor of N-doped and N,K co-doped graphene quantum dots

Chayanee Kaewprom^a, Yonarpach Areerob^b, Won-Chun Oh^b,
Keshav Lalit Ameta^{c,*}, Saksit Chanthai^{a,*}

^a Materials Chemistry Research Center, Department of Chemistry and Center of Excellence for Innovation in Chemistry, Faculty of Science, Khon Kaen University, Khon Kaen 40002, Thailand

^b Department of Advanced Materials Science and Engineering, Hanseo University, 46, Hanseo1ro, Haemi-myun, Seosan, Chungnam, Republic of Korea

^c Department of Chemistry, School of Sciences, Mody University of Science and Technology, Lakshmanagarh 332311, Rajasthan, India

Received 5 October 2019; accepted 31 December 2019

Available online 8 January 2020

KEYWORDS

Graphene quantum dots;
N doped GQDs;
N,K co-doped GQDs;
Fluorescence quenching sensor;
Copper (II);
Mercury (II)

Abstract The present study was aimed to use of N doped graphene quantum dots (N-GQDs) and N,K co-doped graphene quantum dots (N,K-GQDs) as a fluorescence quenching sensor to determine both mercury and copper in water sample, simultaneously using simple fluorescence protocol. Each of N-GQDs or N,K-GQDs was optimized separately with 1–5% (w/v) HNO₃ or KNO₃, respectively, and their quantum yields were determined and compared. It was found that N-GQDs, obtained from 3% (w/v) HNO₃ doped resulted higher fluorescence intensity at the maximum excitation and emission wavelengths of 370 and 460 nm, respectively, with higher quantum yield (QY = 83.42%) compared with that of undoped GQDs (QY = 16.35%). While N,K-GQDs obtained from 5%(w/v) KNO₃ gave somewhat different fluorescence spectrum, but still had the same maximum excitation and emission wavelengths with rather highest QY (94.07%). However, it is interesting that detection sensitivity expressed as slope of their calibration curve ($y = 5.43x - 19.48$; $r^2 = 0.9971$) of the N-GQDs is rather higher than that ($y = 1.29x + 17.66$; $r^2 = 0.9977$) of the N,K-GQDs for Hg²⁺ fluorescence quenching sensor, and the fluorescence intensity of N-GQDs had better selectively quenching effect only by both Hg²⁺ and Cu²⁺. Thus, their quenching effects were selected to develop the fluorescence turn-off sensor for trace level of both metal ions in real water samples. For method validation, the N-GQDs exhibited high sensitivity to detect both Hg²⁺ and Cu²⁺ with wide linear ranges of 20–100 μM and 100–500 μM, respectively. Limit of detection (LOD) and limit of quantitation (LOQ) were 0.42 μM & 1.41 μM for Hg²⁺ and 13.19 μM & 43.97 μM for Cu²⁺, respectively, with their precision expressed as an intra-day and an inter-day analysis of 6.98% & 11.35% for Hg²⁺ and 11.78% & 9.43% for

* Corresponding authors.

E-mail addresses: klameta.cash@modyuniversity.ac.in (K.L. Ameta), sakcha2@kku.ac.th (S. Chanthai).

Cu²⁺, respectively. Also the study of matrix analysis of the water samples (drinking water and tap water), was carried out using N-GQDs and N,K-GQDs resulted good percentage recoveries in comparison with those using undoped GQDs under the same optimum conditions.

© 2020 The Author(s). Published by Elsevier B.V. on behalf of King Saud University. This is an open access article under the CC BY-NC-ND license (<http://creativecommons.org/licenses/by-nc-nd/4.0/>).

1. Introduction

The contamination of heavy metal ions has long been becoming one of the most serious problems in the water quality because of the increasing industrial and agricultural activities as well as the improper release of the metal ions into water resources (Anh et al., 2017; Qi et al., 2017, 2018). Water quality has thus become an issue of vital importance which is the essential resource that has been threatened by pollution. Among the toxic metal ions, mercury ion (Hg²⁺) can be accumulated in vital organs throughout the food chain and cause severe damage to the brain, nervous system, kidney (Chaiyo et al., 2014;), heart and endocrine system. It is the most common and stable form of mercury pollution. Besides natural accumulation of Hg²⁺, its organo species like methyl Hg is also much available and need to be removed from water and fish samples using specific adsorbents under optimum experimental design prior to determination (Tuzen et al., 2009a,b; Saleh et al., 2017; Saleh et al., 2018). At the same time, copper ion (Cu²⁺) can also be harmful, causing irritation of nose and throat, nausea, vomiting and diarrhea (Shoae et al., 2012; Niazi et al., 2015) when the copper content existing too high. Recently, such nanofluid behavior of copper oxide nanoparticles was extensively studied and applied for heat transfer enhancement (Li et al., 2019; Sheikholeslami et al., 2019; Ma et al., 2019). Leaking of Cu²⁺ to contaminate in environmental samples is unavoidably a case study. Therefore, it is rather important to develop a simple, fast and convenient method for simultaneous detection of mercury and copper in such water samples, especially at ultra-trace level analysis.

At present, several methods have been applied for both mercury and copper determination by sophisticated instruments including AAS, ICP-AES, ICP-MS, SERS, GC and LC. However, these methods have a greater cost, higher sample volume requirements and instrumentation complexity limiting. Therefore, this study focuses on the determination of mercury and copper in water sample detecting by simple fluorescence technique. Fluorescence probes working as an effective method to detect the metal ions have been of interest in recent years, which have their advantages much more than those instrumental techniques, giving such as higher sensitivity, specificity, fast response and simple technical procedure (Meng et al., 2018).

More recently besides gold nanoparticles have been used as colorimetric sensor for metal ions detection (Lou et al., 2011), many novel types of fluorescence carbon nanomaterial, graphene quantum dots (GQDs) and/or specific molecular imprinting-based sensors have much been attracted and played more attention (Ding et al., 2016; Yu et al., 2017; Qi et al., 2017; Qi et al., 2018; Q. Yang et al., 2018; Wang et al., 2018a). However, GQDs possess large surface area, small diameter, fine surface grafting using π - π conjugated network or surface functional groups and other special physical properties (Tetsuka et al., 2012; Wang et al., 2014; Wang and Hu, 2014;

Zhu et al., 2012). Its chemical structure contains the carboxyl and hydroxyl groups at their edge enable them to display an excellent water solubility and suitability for successive functionalization with various organic, inorganic, polymeric or biological species (Shen et al., 2011; Shen et al., 2012). GQDs can be tuned by doping elements to increase optical, surface activities and electrical properties of the doped GQDs. Nitrogen atom has been widely used as a dopant as it has a comparable atomic size and five valence electrons to bond carbon atom (Xue et al., 2018). Potassium, K doped GQDs also forms a stable dispersion in water with good crystallinity and uniform diameters (Qian et al., 2016). They show distinctive optical properties comparing with the undoped GQDs.

In this research study, a simple and low-cost synthetic strategy to prepare either N-GQDs or N,K-GQDs by one-pot fusion of solid citric acid with appropriate amounts of concentrate nitric acid or solid potassium nitrate, respectively was carried out. The obtained N-GQDs and N, K-GQDs showed strong fluorescence intensity and high quantum yield (QY) compared with the undoped GQDs. In the presence of Hg²⁺ and Cu²⁺, the fluorescence intensity of both N-GQDs and N, K-GQDs decreases linearly by their quenching mechanism. The interactions between Hg²⁺ or Cu²⁺ and the N-GQDs or N,K-GQDs lead to an electron or an energy transfer from negative charge on the N-GQDs or N, K-GQDs surface to the metal ions. This is thus aimed of using the fluorescence quenching sensor for simultaneous determination of mercury and copper ions with different sensitivity ranges. In addition, the developed analytical method was validated and expressed as their recovery study on applying for both mercury and copper determination in real water samples.

2. Materials and methods

2.1. Chemicals and materials

All the chemicals used were of analytical grade. Citric acid and sodium hydroxide used were from Carlo Erba (Italy). All of selected mineral acids, potassium nitrate, sodium nitrate and sodium acetate were obtained from QRec (New Zealand). Mercury nitrate and copper nitrate trihydrate were purchased from Sigma-Aldrich (Germany). Acetic acid was from Merck (Germany). Potassium dihydrogen phosphate and dipotassium hydrogen phosphate were from LOBA (India). Paraffin oil was brought from Ajex Finechem (Australia). Deionized water (Simplicity Water Purification System, Model Simplicity 185, Millipore, U.S.A.) was used throughout the experiments.

2.2. Instruments and apparatus

Spectrofluorophotometer (Shimadzu RF-5301PC, Japan) with excitation and emission slit widths of 3 nm was mainly used.

pH meter (Model Proline B21, Becthai Equipment & Chemical, Thailand), analytical balance (Model BSA224S-CW, Scientific Promotion, Thailand), quartz cell with 1-cm path length (Fisher Scientific, U.S.A.) were also used. Round bottom flask (Pyrex®, England) and hot plate with a magnetic stirrer in association with paraffin oil bath were set for the citric acid pyrolysis.

2.3. Synthesis and characterization of GQDs and N-GQDs & N,K-GQDs

Graphene quantum dots were prepared by citric acid pyrolysis (Dong et al., 2012). Briefly, 2.0 g citric acid (QRec™, New Zealand) was transferred into a 100 mL round bottom flask which was heated to 250 °C in an oil bath for about 5 min. Citric acid was liquated and its color was changed rapidly to yellow. This liquid was then dissolved by dropwise addition of 100 mL 0.25 M NaOH (QRec™, New Zealand) with continuous stirring for 30 min. The obtained GQDs solution was stored at 4 °C before use. For N-GQDs or N,K doped GQDs synthesis, the GQDs, as also prepared via citric acid pyrolysis, were simultaneously treated with 1–5% (w/v) nitric acid (QRec™, New Zealand) or 1–5% (w/v) potassium nitrate (QRec™, New Zealand) to find the suitable amount of N or N,K doping condition; starting with 2.0 g of citric acid and 1% (w/v) nitric acid or 1% (w/v) potassium nitrate was transferred into a 100 mL round bottom flask, which was heated to 250 °C in an oil bath for about 5 min and then each of the two mixture solutions was dissolved in 100 mL 0.25 M NaOH solution as mentioned above. The as-prepared N-GQDs and N,K-GQDs solution were also stored at 4 °C before use.

2.4. Quantum yield measurement

Determination of the fluorescence quantum yield (QY) of undoped GQDs, N-GQDs and N,K-GQDs was carried out by comparing with standard solution of quinine sulfate (QY = 0.54 at 360 nm) used as a reference compound. The quantum yield is calculated using the slope of the regression line generated by plotting the integrated fluorescence intensity at the emission wavelength of 460 nm against with its absorbance at 370 nm for multiple concentrations of each of undoped GQDs, N-GQDs and N,K-GQDs, and quinine sulfate solutions. The QY was calculated by the following equation (Amini et al., 2017):

$$Q = Q_R \times [m/m_R] \times [n^2/n_R^2]$$

where, Q is the quantum yield, m is the slope of the mentioned regression line, n is refractive index that assuming equal to 1.33 for both solution and the subscript R refers to quinine sulfate solution.

2.5. Selective fluorescence quenching detection of Hg²⁺ and Cu²⁺ using N-GQDs & N,K-GQDs

For these following experiments, about 100 mg/L of each GQDs, N-GQDs or N,K-GQDs solution and 0.1 M phosphate buffer solution pH 7 were mixed well in a 10 mL volumetric flask. Then various concentrations of each of Hg²⁺ and Cu²⁺ were added into an aliquot of each of undoped GQDs,

N-GQDs or N,K-GQDs solution (10 mL final volume). These Hg²⁺ and Cu²⁺ quenching fluorescence spectra of each of the undoped GQDs, N-GQDs or N,K-GQDs solution were recorded immediately at $\lambda_{ex}/\lambda_{em}$ 370/460 nm. Then, the spectral measurements were used to plot the quenching external calibration curve for both Hg²⁺ and Cu²⁺ with different concentration ranges.

2.6. Recovery study of real water samples

To evaluate the undoped GQDs, N-GQDs and N,K-GQDs based fluorescence quenching sensor for Hg²⁺ and Cu²⁺ detection simultaneously in an artificial solution, the applicability of the proposed method for real water samples including drinking water and tap water was carried out. Tap water samples were collected with polyethylene bottle from Khon Kaen area and were analyzed without any pretreatment. All water samples were filtered through Whatman filter paper No.42 and then adjusted to pH 7 with 0.1 M phosphate buffer. In this procedure, 1 mL of the water sample and 0.5 mL of undoped GQDs, N-GQDs or N,K-GQDs (100 mg/L) solution were transferred into 10.0 mL volumetric flask. Then, each of the sample mixture was spiked with three concentration levels of standard solution of Hg²⁺ (20.0, 50.0 and 100.0 µM) and standard solution of Cu²⁺ (100.0, 300.0 and 500.0 µM).

2.7. Statistical analysis

Regarding statistical data analysis in an analytical method validation, statistics for those experimental results obtained at least in triplicate include mean, standard deviation, confidence intervals, and linear regression. Data analysis and their curve fitting using all registered statistical packages as such common Excel 2016 is reported.

3. Results and discussion

3.1. FT-IR characterization of the undoped GQDs, N-GQDs & N,K-GQDs

The FTIR spectra of undoped GQDs, N-GQDs and N,K-GQDs are shown in Fig. 1(a)–(c). From the vibration spectrum of undoped GQDs (Fig. 1(a)), the absorption peaks at 3436, 2950, 1576 and 1080 cm⁻¹ were observed, indicating the vibration modes of hydroxyl stretching, C–H stretching, C=C stretching of polycyclic aromatic hydrocarbons (Wang et al., 2014), C–O in COH/COC (epoxy) groups (Wang et al., 2009), respectively. These results confirm the undoped GQDs successfully synthesized by citric acid pyrolysis. The FTIR spectrum of N-GQDs is shown in Fig. 1(b), with the broad band at 3000 – 3500 cm⁻¹ corresponding to the stretching vibrations of O–H and N–H (Kaur et al., 2017; Mondal et al., 2018). The absorption peaks at ~1700, 1585 and 1218 cm⁻¹ indicate C=C, C=O and C–O–C stretching vibrations, respectively. Surprisingly, the IR spectrum peak at ~1400 cm⁻¹ was from the vibration mode of C–NH, indicating that the successful doped of nitrogen atom onto the surface of GQDs (Ju and Chen, 2014; C. Zhang et al., 2016). Furthermore, Fig. 1(c) shows an additional peak at 1777 cm⁻¹ for the N,K-GQDs, which is probably resulted from potassium

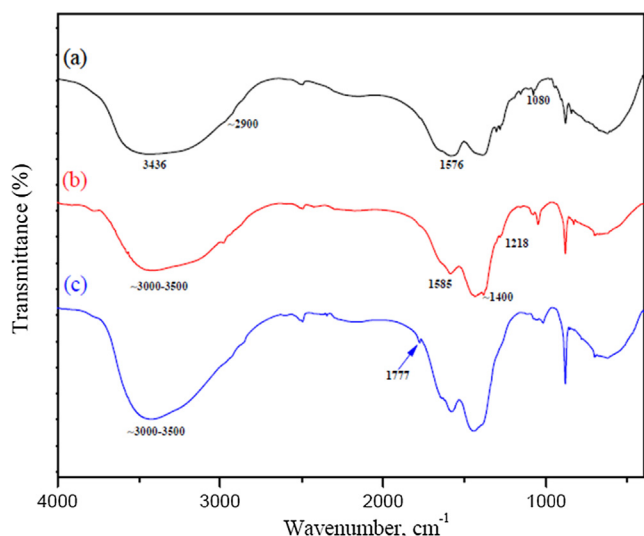


Fig. 1 FT-IR Spectra of (a) GQDs, (b) N-GQDs and (c) N,K-GQDs.

related bonding (Qian et al., 2016; Ain et al., 2016). Therefore, these FTIR spectra can be commonly used to confirm their chemical structures of the as-prepared N-GQDs and N,K-doped GQDs.

3.2. Effect of mineral acids on GQDs yield

For preliminary study, fluorescence spectra of both undoped GQDs and GQDs doped with some mineral acids are shown in Fig. 2. Their absorption spectra were found around 370 nm. When the mineral acids were thermally degraded and decorated into the defaulted surface structure of the GQDs by pyrolysis situation, their emission spectra appeared nearly around 460 nm with either an enhanced or quenched fluorescence process. Thus confirming that the mineral acids

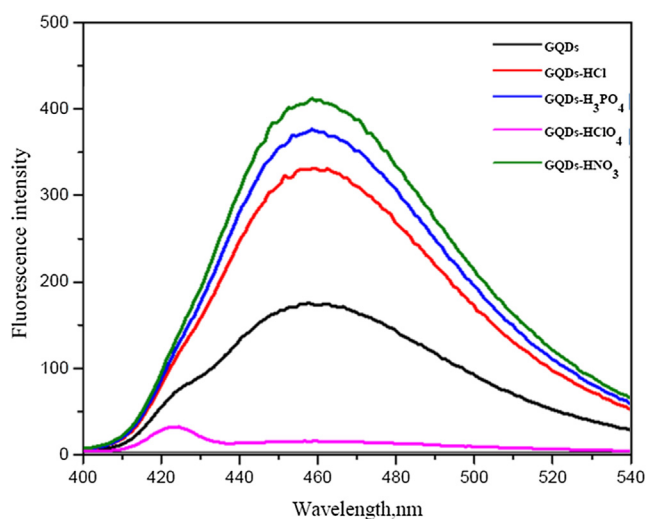


Fig. 2 Fluorescence spectra of GQDs (black) and 1% (w/v) each of some mineral acids doped with GQDs (nitric acid/GQDs – green; phosphoric acid/GQDs – blue; hydrochloric acid/GQDs – red; perchloric acid/GQDs – violet).

doping in the GQDs was successfully obtained and such GQDs doped with nitric acid (HNO_3) was chosen as the starting material because of much higher fluorescence intensity. The enhancing fluorescence emission of GQDs doped with HNO_3 possibly resulted from the N-doping induced modification of the chemical and electronic characteristics of the GQDs (Liu et al., 2018; Cai et al., 2014; Wang and Fan, 2018).

3.3. Quenching effect of metal ions on the fluorescence intensity of N-GQDs

The effect of some metal ions including Ag^+ , Na^+ , Hg^+ , Cu^{2+} , Pb^{2+} , Mn^{2+} , Mg^{2+} , Fe^{2+} , Fe^{3+} and Al^{3+} ions on the fluorescence intensity of the N-GQDs was tested. The fluorescence intensity and the normalized fluorescence intensity of N-GQDs solution showed the quenching effect with adding Hg^{2+} (Fig. 3(a)) and Cu^{2+} (Fig. 3(b)). Hg^{2+} can interact with negative charge on the surface of N-GQDs because of their electrostatic interactions on the quenching process. Some metal ions such as Cu^{2+} can also interact with negative charge on the surface of N-GQDs but their ion bindings are somewhat weak and its binding affinity is not much as strong as that of the Hg^{2+} (Li et al., 2015). Therefore, the quenching process of Cu^{2+} would be weaker than that of Hg^{2+} . The quenching processes of both Hg^{2+} and Cu^{2+} on the surface of N-GQDs are considerably due to facilitating non-radiative electron/hole recombination annihilation through an effective electron transfer (Huang et al., 2013; Liu et al., 2016; He et al., 2016). The electron transfers from the excited state of N-GQDs to an empty d -orbital of the metal ion lead to the fluorescence quenching effect of the N-GQDs.

3.4. Selective detection of Hg^{2+} and Cu^{2+} using N-GQDs

The fluorescence intensities of N-GQDs increased with the increase in HNO_3 concentration (Fig. 4). The enhancement of fluorescence intensity would be due to the emissive traps of the nitrogen doped on the surface of GQDs. The nitrogen atom is comparable in an atomic size to the carbon atom and their effects turn on the electronic nature of GQDs due

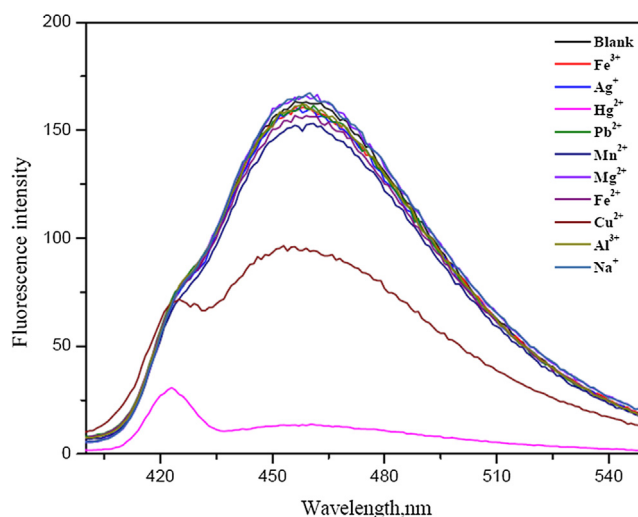


Fig. 3a Fluorescence spectra of 1% (w/v) HNO_3 doped GQDs in the presence of various metal ions

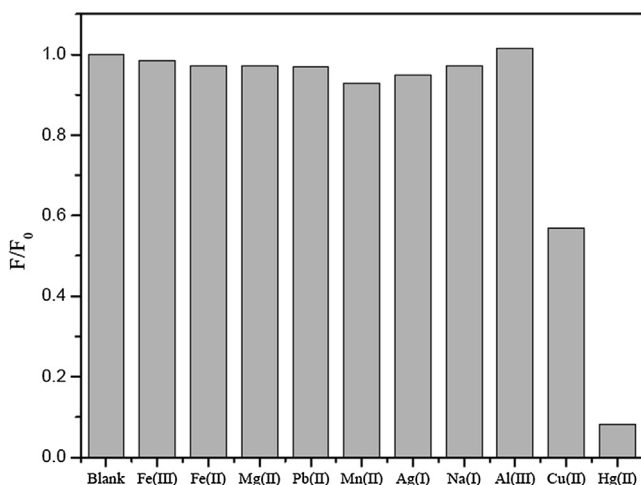


Fig. 3b Normalized fluorescence intensities of 1% (w/v) HNO₃ doped GQDs in the presence of various metal ions

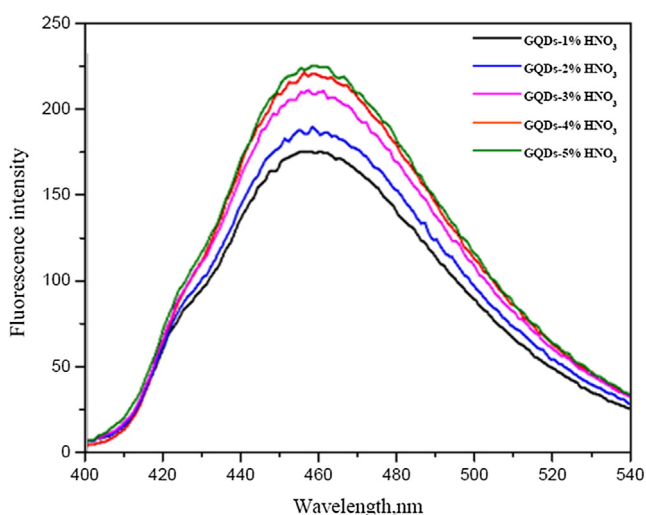


Fig. 4 Fluorescence spectra of GQDs and 1–5% (w/v) HNO₃ doped GQDs

to difference in an electronegativity between C and N that appears large enough to result in significant charge transfer in the C-N composites (Chen et al., 2017). Therefore, the chemical doping of nitrogen atom into the framework of GQDs would directly be attributed. Figs. 5 and 6 show such calibration curves plotting between $F_0 - F$ and concentrations of Hg²⁺ and Cu²⁺ (μM) using GQDs doped with 1 to 5% (w/v) of HNO₃. It was shown that their slopes between 20–200 μM of Hg²⁺ and slopes between 100–500 μM of Cu²⁺ were found linearly increasing with the percentage of nitric acid used, of which their calibration curves of GQDs doped with 3% and 5% (w/v) nitric acid gave higher sensitivity to detect both Hg²⁺ and Cu²⁺, respectively.

Fig. 7 shows the fluorescence spectra of GQDs doped with potassium nitrate. The results showed the fluorescence spectrum is rather difference in shape from that of the N-GQDs, and their intensities also increased with the increase in KNO₃ concentrations. So, GQDs doped with this nitrate salt

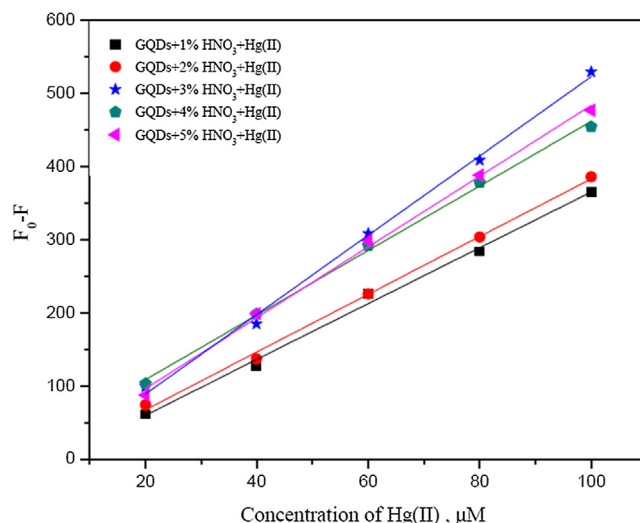


Fig. 5 Calibration curves plotting between $F_0 - F$ and concentrations of Hg²⁺ (μM) using GQDs doped with 1–5% (w/v) HNO₃

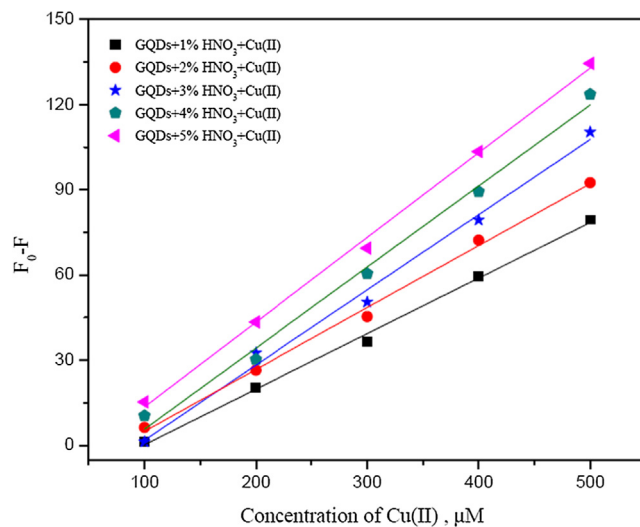


Fig. 6 Calibration curves plotting between $F_0 - F$ and concentrations of Cu²⁺ (μM) using GQDs doped with 1–5% (w/v) HNO₃

may has distinct chemical structure, the so-called N,K-GQDs form. The enhancement of their fluorescence intensity would due to attribution in between π and π^* orbital of the N,K-GQDs (C. Zhang et al., 2016; Ain et al., 2016). The change in energy structure would therefore lead to the change in their optical properties as well.

Also, the N,K-GQDs can be used to detect both Hg²⁺ and Cu²⁺ as shown in Figs. 8 and 9. The calibration curves show that their slopes between 20–200 μM for Hg²⁺ and 100–500 μM for Cu²⁺ increase with increasing the percentage of potassium nitrate, of which the calibration curve of GQDs doped with 5% (w/v) KNO₃ give higher sensitivity to detect both of Hg²⁺ and Cu²⁺.

The strong fluorescence intensity of N-GQDs and N,K-GQDs was also investigated by using quinine sulfate solution as a reference case. The quantum yields of different doping materials are compiled in Table 1. The fluorescence quantum

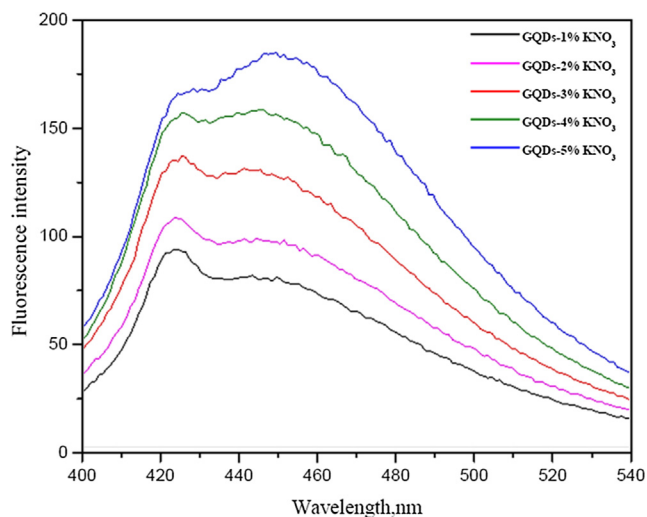


Fig. 7 Fluorescence spectra of GQDs and 1–5% (w/v) KNO_3 doped GQDs

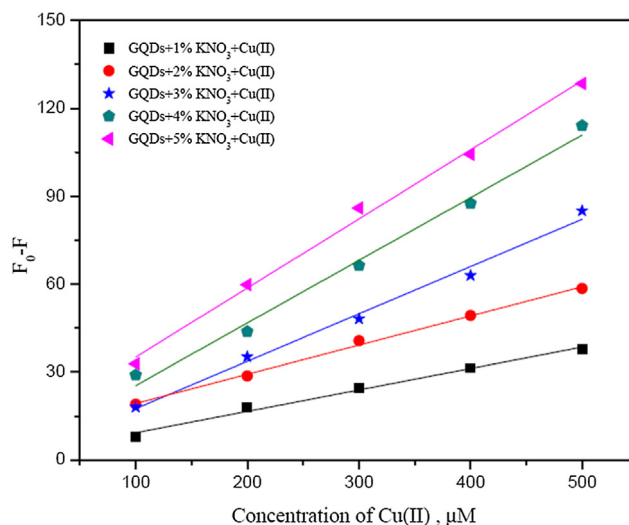


Fig. 9 Calibration curves plotting between $F_0 - F$ and concentrations of Cu^{2+} (μM) using GQDs doped with 1–5% (w/v) KNO_3

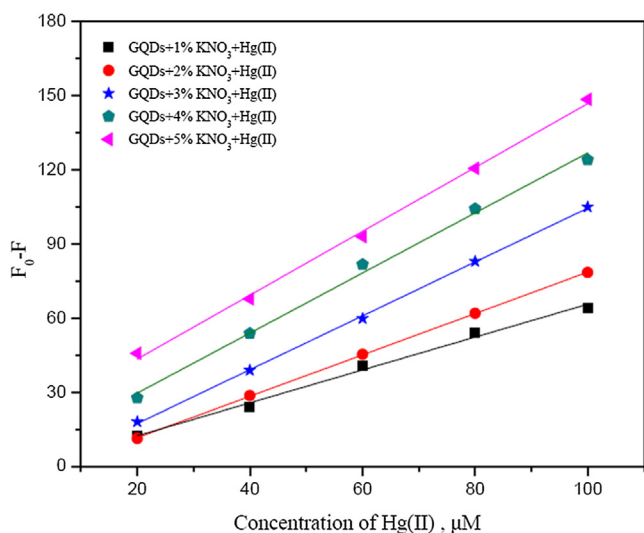


Fig. 8 Calibration curves plotting between $F_0 - F$ and concentrations of Hg^{2+} (μM) using GQDs doped with 1–5% (w/v) KNO_3

yields of the obtained N-GQDs and N,K-GQDs was found to be 83.42% and 94.07%, respectively, which they were higher than that of the undoped GQDs and quinine sulfate, so the doping N and K on the surface of GQDs gave significant enhancement of the fluorescence quantum yields of the GQDs (Yan et al., 2016).

Comparison of detection sensitivity for Hg^{2+} and Cu^{2+} in terms of their slopes of its calibration curves using the undoped GQDs, N-GQDs and N,K-GQDs as fluorescence quenching sensor is shown in Table 2. Thus, quantitative analysis of both Hg^{2+} and Cu^{2+} was validated and their analytical parameters were listed in Table 3. The fluorescence intensity of the optimal N-GQDs decreased with an increasing in concentrations from 20 to 100 μM of Hg^{2+} and 100 to 500 μM of Cu^{2+} . Both limit of detection (LOD) and limit of quantitation (LOQ) of the proposed fluorescence quenching sensor were 0.42 μM & 1.41 μM for Hg^{2+} , and 13.2 μM & 44.0 μM for

Table 1 Quantum yield of undoped GQDs, N-GQDs and N,K-GQDs with respect to quinine sulfate.

Material/chemical	Quantum yield (%)
Undoped GQDs	16.35
N-GQDs from 3% (w/v) HNO_3 doped	83.42
N,K-GQDs from 5% (w/v) KNO_3 doped	94.07
Quinine sulfate	54.00

Table 2 Comparison of detection sensitivity for Hg^{2+} and Cu^{2+} in terms of their slopes of its calibration curves using undoped GQDs, N-GQDs and N,K-GQDs as fluorescence quenching sensor.

Material	20–100 μM Hg^{2+}	100–500 μM Cu^{2+}
Undoped GQDs	$y = 1.43x + 8.66$; $r^2 = 0.9982$	$y = 0.18x - 20.72$; $r^2 = 0.9841$
N-GQDs	$y = 5.43x - 19.48$; $r^2 = 0.9971$	$y = 0.30x - 16.24$; $r^2 = 0.9977$
N,K-GQDs	$y = 1.29x + 17.66$; $r^2 = 0.9977$	$y = 1.18x + 11.49$; $r^2 = 0.9958$

Cu^{2+} , respectively. The intra-day precision and inter-day precision expressed as the percentage of RSDs were 6.98 and 11.35 for Hg^{2+} , and 11.78 and 9.43 for Cu^{2+} , respectively, derived from the detection of the solution model of 40.0 μM Hg^{2+} and 300.0 μM Cu^{2+} . These results suggest that the proposed method exhibits a very good repeatability and is therefore acceptable for simultaneous determination of Hg^{2+} and Cu^{2+} with different sensitivity ranges in the same sample solution.

The proposed protocol was applied for Hg^{2+} and Cu^{2+} determination in drinking water and tap water samples. From the results (Tables 4–6), their recoveries of the spiked Hg^{2+} and Cu^{2+} by using undoped GQDs were obtained in the ranges of $96.75 \pm 2.88 - 104.95 \pm 6.01\%$ and $96.38 \pm 6.18 - 106.30 \pm 7.06\%$, respectively. The recoveries when using

Table 3 Calibration curve, limit of detection (LOD), limit of quantitation (LOQ), and repeatability of the method validation using N-GQDs as a fluorescence quenching sensor.

Metal ion	Calibration curve* (μM)	r^2	LOD (μM)	LOQ (μM)	Intra-day analysis (%)	Inter-day analysis (%)
Hg^{2+}	20–100	0.9949	0.42	1.41	6.98	11.35
Cu^{2+}	100–500	0.9727	13.2	44.0	11.78	9.43

* Linear equations for Hg^{2+} $y = 5.16x - 19.15$ and for Cu^{2+} $y = 0.28x - 15.04$.

N-GQDs were found in the ranges of $99.00 \pm 1.29 - 101.25 \pm 1.66\%$ for Hg^{2+} and $99.06 \pm 2.06 - 101.73 \pm 0.65\%$ for Cu^{2+} , while the recoveries obtained from using N,K-GQDs were also in the ranges of $95.75 \pm 7.11 - 102.75 \pm 2.39\%$ for Hg^{2+} and $97.32 \pm 7.17 - 101.10 \pm 5.55\%$ for Cu^{2+} . This method evaluation is very satisfactorily attributed in terms of an analytical accuracy of the trace metal detection. However, comparison of different fluorescence sensing considered as LOD for Hg^{2+} and Cu^{2+} detection is complied. Even though its sensitivity of N-GQDs probe for Hg^{2+} detection is

a little bit higher when compared with other literatures, it might be due to differences in optimum conditions used under specific detection studied. In such case of Cu^{2+} detection using N-GQDs sensing probe it is still limited. Therefore, this study is aimed to report the use of N-GQDs as fluorescence sensing probe for simultaneous detection of both Hg^{2+} and Cu^{2+} existing in the same sample solution with different sensitivity range as mentioned above. It is concluded that the proposed method can be successfully applied to real water samples including drinking water and tap water [Table 7](#).

Table 4 Recoveries of Hg^{2+} and Cu^{2+} spiked in real water samples using undoped GQDs ($n = 3$).

Water sample	Hg^{2+}			Cu^{2+}		
	Added (μM)	Found (μM)	Recovery (%) \pm SD	Added (μM)	Found (μM)	Recovery (%) \pm SD
Drinking water 1	20.00	20.11	102.75 ± 4.25	100.00	100.13	102.05 ± 2.98
	60.00	60.04	100.16 ± 3.21	300.00	300.06	100.31 ± 3.78
	100.00	99.85	99.25 ± 5.74	500.00	499.13	97.26 ± 4.41
Drinking water 2	20.00	20.09	101.45 ± 5.05	100.00	100.06	100.94 ± 4.00
	60.00	60.08	100.66 ± 2.25	300.00	300.08	100.41 ± 6.74
	100.00	100.10	100.50 ± 2.59	500.00	500.12	100.38 ± 2.50
Drinking water 3	20.00	19.64	98.50 ± 4.55	100.00	99.87	97.95 ± 4.18
	60.00	59.99	99.91 ± 2.64	300.00	299.94	100.73 ± 4.35
	100.00	100.23	101.15 ± 3.30	500.00	500.21	100.66 ± 2.24
Tap water 1	20.00	19.87	96.75 ± 2.88	100.00	100.40	106.30 ± 7.06
	60.00	59.98	99.83 ± 3.17	300.00	300.02	100.10 ± 4.95
	100.00	100.71	103.55 ± 5.11	500.00	499.96	99.87 ± 4.84
Tap water 2	20.00	19.90	97.50 ± 7.05	100.00	99.62	96.38 ± 6.18
	60.00	60.03	100.25 ± 7.87	300.00	299.96	100.26 ± 6.35
	100.00	100.99	104.95 ± 6.01	500.00	500.54	101.10 ± 3.58

Table 5 Recoveries of Hg^{2+} and Cu^{2+} spiked in real water samples using N-GQDs ($n = 3$).

Water sample	Hg^{2+}			Cu^{2+}		
	Added (μM)	Found (μM)	Recovery (%) \pm SD	Added (μM)	Found (μM)	Recovery (%) \pm SD
Drinking water 1	20.00	20.01	100.25 ± 1.11	100.00	99.99	99.84 ± 1.56
	60.00	60.05	100.41 ± 0.78	300.00	300.03	100.16 ± 0.54
	100.00	100.10	100.50 ± 0.59	500.00	500.02	100.06 ± 1.22
Drinking water 2	20.00	20.04	101.00 ± 1.02	100.00	100.04	100.63 ± 1.34
	60.00	60.10	100.00 ± 0.96	300.00	300.45	101.57 ± 0.89
	100.00	100.01	100.05 ± 0.68	500.00	500.01	100.03 ± 1.19
Drinking water 3	20.00	10.99	99.75 ± 1.01	100.00	100.05	100.78 ± 0.97
	60.00	60.00	100.00 ± 0.47	300.00	300.33	101.73 ± 0.65
	100.00	100.04	100.20 ± 0.97	500.00	500.06	100.19 ± 1.01
Tap water 1	20.00	20.05	101.25 ± 1.66	100.00	100.08	99.06 ± 2.06
	60.00	60.13	100.00 ± 0.98	300.00	299.95	100.41 ± 1.89
	100.00	100.22	101.10 ± 1.03	500.00	499.95	99.84 ± 0.99
Tap water 2	20.00	19.96	99.00 ± 1.29	100.00	99.97	99.52 ± 1.11
	60.00	60.11	100.92 ± 1.03	300.00	300.05	100.26 ± 2.78
	100.00	100.12	100.60 ± 0.89	500.00	500.23	100.72 ± 2.87

Table 6 Recoveries of Hg²⁺ and Cu²⁺ spiked in real water samples using N,K-GQDs (n = 3).

Water sample	Hg ²⁺			Cu ²⁺		
	Added (μM)	Found (μM)	Recovery (%) ± SD	Added (μM)	Found (μM)	Recovery (%) ± SD
Drinking water 1	20.00	20.11	102.75 ± 2.39	100.00	100.07	101.10 ± 5.55
	60.00	60.08	100.67 ± 4.87	300.00	300.08	100.42 ± 2.98
	100.00	99.86	99.30 ± 6.02	500.00	499.41	98.14 ± 3.89
Drinking water 2	20.00	20.08	102.00 ± 5.11	100.00	100.04	100.63 ± 5.12
	60.00	60.02	100.17 ± 2.88	300.00	300.05	100.26 ± 3.58
	100.00	100.21	101.05 ± 2.91	500.00	500.07	100.22 ± 7.41
Drinking water 3	20.00	9.89	97.25 ± 6.55	100.00	99.97	99.06 ± 3.58
	60.00	60.01	100.08 ± 4.51	300.00	300.04	100.21 ± 2.98
	100.00	100.12	100.60 ± 4.37	500.00	500.14	100.44 ± 4.97
Tap water 1	20.00	9.83	95.75 ± 7.11	100.00	99.83	97.32 ± 7.17
	60.00	59.96	99.67 ± 6.34	300.00	300.05	100.26 ± 6.62
	100.00	100.48	102.40 ± 5.01	500.00	500.14	100.44 ± 5.11
Tap water 2	20.00	19.85	96.25 ± 6.47	100.00	99.86	97.80 ± 6.28
	60.00	60.13	101.08 ± 6.40	300.00	300.11	100.58 ± 7.47
	100.00	100.41	102.05 ± 4.12	500.00	500.26	100.82 ± 4.17

Table 7 Comparison of different fluorescence sensing expressed as LOD for Hg²⁺ and Cu²⁺ detection.

Material probe	Hg ²⁺	Cu ²⁺	Reference
GQDs	0.43 nM	–	Z. Li et al. (2015)
N-GQDs	1.3 nM	–	Z. Liu et al. (2016)
N-CQDs	1.48 nM	–	Y. Zhang et al. (2016)
N-GQDs	67.3 nM	–	Y. Yang et al. (2019)
N-GQDs	0.10 μM	–	Wang et al., 2018a
N-GQDs	0.42 μM	13.2 μM	This work

4. Conclusion

A simple and low-cost procedure for one-pot synthesis of N-GQDs and N,K-GQDs was emphasized and successfully developed using pyrolysis of solid citric acid with either concentrate nitric acid or potassium nitrate. The advantages of the proposed method were as following (1) both N-GQDs and N,K-GQDs show strong fluorescence intensity and give higher quantum yields compared with its undoped GQDs, (2) the N-GQDs and N,K-GQDs both give high sensitive and selective determination of Hg²⁺ and Cu²⁺, (3) their fluorescence intensity decreases linearly by quenching mechanism, and (4) the detection of Hg²⁺ and Cu²⁺ was achieved with fast response, wide linear range, rather lower detection limit and can be applied to real water samples without any matrix interference. The novelty of the N-GQDs or N,K-GQDs can easily be implied for routine analysis of simultaneous detection of the two metal ions under the selected optimal conditions with satisfactorily analytical figures of merit and, in-turn, would serve as a friendly eco-environmental green chemistry.

Conflict of Interest declaration

Authors have no conflict of interest.

Acknowledgements

The authors are thankful to the Materials Chemistry Research Center, Department of Chemistry and Center of Excellence for

Innovation in Chemistry (PERCH-CIC), Khon Kaen University for financial support. Authors are also thankful to School of Sciences, Mody University of Science and Technology for providing necessary support to complete this study.

References

- Meng, A., Xu, Q., Zhao, K., Li, Z., Liang, J., Li, Q., 2018. A highly selective and sensitive “on-off-on” fluorescent probe for detecting Hg(II) Based on Au/N-doped carbon quantum dots. *Sens. Actuators, B* 255, 657.
- Niazi, A., Habibi, S., Ramezani, M., 2015. Preconcentration and simultaneous spectrophotometric determination of copper and mercury by dispersive liquid–liquid microextraction and orthogonal signal correction–partial least squares. *Arab. J. Chem.* 8, 706. <https://doi.org/10.1016/j.arabjc.2013.12.014>.
- Zhang, C., Cui, Y., Song, L., Liu, X., Hu, Z., 2016a. Microwave assisted one-pot synthesis of graphene quantum dots as highly sensitive fluorescent probes for detection of iron ions and pH value. *Talanta* 150, 54. <https://doi.org/10.1016/j.talanta.2015.12.015>.
- Wang, C.-X., Sun, Y., Jin, J., Xiong, Z., Li, D., Yao, J., Liu, Y., 2018a. Highly selective, rapid-functioning and sensitive fluorescent test paper based on graphene quantum dots for on-line detection of metal ions. *Anal. Methods* 10, 1163. <https://doi.org/10.1039/C7AY02995K>.
- Cai, F., Liu, X., Liu, S., Liu, H., Huang, Y., 2014. A simple one-pot synthesis of highly fluorescent nitrogen-doped graphene quantum dots for the detection of Cr(VI) in aqueous media. *RSC Adv.* 4, 52016. <https://doi.org/10.1039/C4RA09320H>.
- Li, F., Sheikholeslami, M., Dara, R.N., Jafaryar, M., Shafee, A., Nguyen-Thoi, T., Li, Z., 2019. Numerical study for nanofluid behavior inside a storage finned enclosure involving melting process. *J. Mol. Liq.*, 111939. <https://doi.org/10.1016/j.molliq.2019.111939>.
- Qian, F., Li, X., Tang, L., Lai, S.K., Lu, C., Lau, S.P., 2016. Potassium doping: tuning the optical properties of graphene quantum dots. *AIP Adv.* 6 (7), 075116. <https://doi.org/10.1063/1.4959906>.
- Huang, H., Liao, L., Xu, X., Zou, M., Liu, F., Li, N., 2013. The electron-transfer based interaction between transition metal ions and photoluminescent graphene quantum dots (GQDs): a platform for metal ion sensing. *Talanta* 117, 152–157. <https://doi.org/10.1016/j.talanta.2013.08.055>.
- Shoae, H., Roshdi, M., Khanlarzadeh, N., Beiraghi, A., 2012. Simultaneous preconcentration of copper and mercury in water

- samples by cloud point extraction and their determination by inductively coupled plasma atomic emission spectrometry. *Spectrochim. Acta Part A Mol. Biomol. Spectrosc.* 98, 70. <https://doi.org/10.1016/j.saa.2012.08.027>.
- Tetsuka, H., Asahi, R., Nagoya, A., Okamoto, K., Tajima, I., Ohta, R., Okamoto, A., 2012. Optically tunable amino-functionalized graphene quantum dots. *Adv. Mater.* 24 (39), 5333–5338. <https://doi.org/10.1002/adma.201201930>.
- Wang, H., Hao, Q., Yang, X., Lu, L., Wang, X., 2009. Graphene oxide doped polyaniline for supercapacitors. *Electrochem. Commun.* 11, 1158. <https://doi.org/10.1016/j.elecom.2009.03.036>.
- He, J., Zhang, H., Zou, J., Liu, Y., Zhuang, J., Xiao, Y., Lei, B., 2016. Carbon dots-based fluorescent probe for “off-on” sensing of Hg(II) and I⁻. *Biosens. Bioelectron.* 79, 531. <https://doi.org/10.1016/j.bios.2015.12.084>.
- Ju, J., Chen, W., 2014. Synthesis of highly fluorescent nitrogen-doped graphene quantum dots for sensitive, label-free detection of Fe (III) in aqueous media. *Biosens. Bioelectron.* 58, 219–225. <https://doi.org/10.1016/j.bios.2014.02.061>.
- Qi, Ji, Li, Bowei, Wang, Xinran, Zhang, Zhong, Wang, Zhuo, Han, Jinglong, Chen, Lingxin, 2017. Three-dimensional paper-based microfluidic chip device for multiplexed fluorescence detection of Cu²⁺ and Hg²⁺ ions based on ion imprinting technology. *Sens. Actuators, B* 251, 224–233. <https://doi.org/10.1016/j.snb.2017.05.052>.
- Qi, J., Li, B., Wang, X., Fu, L., Luo, L., Chen, L., 2018. Rotational paper-based microfluidic-chip device for multiplexed and simultaneous fluorescence detection of phenolic pollutants based on a molecular-imprinting technique. *Anal. Chem.* 90, 11827. <https://doi.org/10.1016/acs.analchem.8b01291>.
- Shen, J., Zhu, Y., Chen, C., Yang, X., Li, C., 2011. Facile preparation and upconversion luminescence of graphene quantum dots. *Chem. Commun.* 47 (9), 2580–2582. <https://doi.org/10.1039/C0CC04812G>.
- Shen, J., Zhu, Y., Yang, X., Zong, J., Zhang, J., Li, C., 2012. One-pot hydrothermal synthesis of graphene quantum dots surface-passivated by polyethylene glycol and their photoelectric conversion under near-infrared light. *New J. Chem.* 36 (1), 97–101. <https://doi.org/10.1039/C1NJ20658C>.
- Yu, J., Wang, X., Kang, Q., Li, J., Shen, D., Chen, L., 2017. One-pot synthesis of quantum dots-based molecular imprinting nanosensor for highly selective and sensitive fluorescence detection of 4-nitrophenol in environmental waters. *Environ. Sci. Nano* 4, 493. <https://doi.org/10.1039/c6en00395h>.
- Chen, L., Wu, C., Du, P., Feng, X., Wu, P., Cai, C., 2017. Electrolyzing synthesis of boron-doped graphene quantum dots for fluorescence determination of Fe³⁺ ions in water samples. *Talanta* 164, 100. <https://doi.org/10.1016/j.talanta.2016.11.019>.
- Amini, M.H., Faridbod, F., Ganali, M.R., Norouzi, P., 2017. Functionalized graphene quantum dots as a fluorescent “off-on” nanosensor for detection of mercury and ethyl xanthate. *Res. Chem. Intermed.* 43, 7457. <https://doi.org/10.1007/s11164-017-3086-1>.
- Kaur, M., Mehta, S.K., Kansal, S.K., 2017. A fluorescent probe based on nitrogen doped graphene quantum dots for turn off sensing of explosive and detrimental water pollutant, TNP in aqueous medium. *Spectrochim. Acta Part A Mol. Biomol. Spectrosc.* 180, 37–43. <https://doi.org/10.1016/j.saa.2017.02.035>.
- Sheikholeslami, M., Resaeianjouybari, B., Darzi, M., Shafee, A., Li, Z., Nguyen, T.K., 2019. Application of nano-refrigerant for boiling heat transfer enhancement employing an experimental study. *Inter. J. Heat Mass Transf.* 141, 974. <http://10.1016/j.ijheatmasstransfer.2019.07.043>.
- Tuzen, M., Uluzlu, O.D., Karaman, I., Soylak, M., 2009a. Mercury (II) and mercury speciation on *Streptococcus pyogenes* loaded Dowex Optipore SD-2. *J. Hazard. Mat.* 169 (1–3), 345. <https://doi.org/10.1016/j.jhazmat.2009.03.100>.
- Tuzen, M., Karaman, I., Citak, D., Soylak, M., 2009b. Mercury(II) and methyl mercury determinations in water and fish samples by using solid phase extraction and cold vapour atomic absorption spectrometry combination. *Food Chem. Toxic.* 47, 1648. <https://doi.org/10.1016/j.fct.2009.04.024>.
- Anh, N.T.N., Chowdhury, A.D., Doong, R.-A., 2017. Highly sensitive and selective detection of mercury ions using N, S-codoped graphene quantum dots and its paper strip based sensing application in wastewater. *Sens. Actuators, B* 252, 1169. <https://doi.org/10.1016/j.snb.2017.07.177>.
- Ain, N.-U., Eriksson, M.O., Schmidt, S., Asghar, M., Lin, P.-C., Holtz, P.O., Syvaarvi, M., Yazdi, G.R., 2016. Tuning the emission energy of chemically doped graphene quantum dots. *Nanomaterials* 6, 198. <https://doi.org/10.3390/nano6110198>.
- Yang, Q., Li, J., Wang, X., Peng, H., Xiong, H., Chen, L., 2018. Strategies of molecular imprinting-based fluorescence sensors for chemical and biological analysis. *Biosens. Bioelectron.* 112, 54. <https://doi.org/10.1016/j.bios.2018.04.028>.
- Chaiyo, S., Chailapakul, O., Siangproh, W., 2014. Highly sensitive determination of mercury using copper enhancer by diamond electrode coupled with sequential injection-anodic stripping voltammetry. *Anal. Chim. Acta* 852, 55. <https://doi.org/10.1016/j.aca.2014.09.011>.
- Zhu, S., Tang, S., Zhang, J., Yang, B., 2012. Control the size and surface chemistry of graphene for the rising fluorescent materials. *Chem. Commun.* 48, 4527. <https://doi.org/10.1039/C2CC31201H>.
- Saleh, T.A., Sari, A., Tuzen, M., 2017. Optimization of parameters with experimental design for the adsorption of mercury using polyethylenimine modified-activated carbon. *J. Environ. Chem. Eng.* 5 (1), 1079. <https://doi.org/10.1016/j.jece.2017.01.032>.
- Saleh, T.A., Tuzen, M., Sari, A., 2018. Polyamide magnetic palygorskite for the simultaneous removal of Hg(II) and methyl mercury; with factorial design analysis. *J. Environ. Manage.* 211, 323. <https://doi.org/10.1016/j.jenvman.2018.01.050>.
- Lou, T., Chen, Z., Wang, Y., Chen, L., 2011. Blue-to-red colorimetric sensing strategy for Hg²⁺ and Ag⁺ via redox-regulated surface chemistry of gold nanoparticles. *ACS Appl. Mat Interf.* 3, 1568. <https://doi.org/10.1021/am200130e>.
- Mondal, T.K., Dinda, D., Saha, S.K., 2018. Nitrogen, sulphur co-doped graphene quantum dot: an excellent sensor for nitroexplosives. *Sens. Actuators, B* 257, 586. <https://doi.org/10.1016/j.snb.2017.11.012>.
- Liu, X., Na, W., Liu, Q., Su, X., 2018. A novel label-free fluorescent sensor for highly sensitive detection of bleomycin based on nitrogen-doped graphene quantum dots. *Anal. Chim. Acta* 1028, 45. <https://doi.org/10.1016/j.aca.2018.04.038>.
- Ma, X., Sheikholeslami, M., Jafaryar, M., Shafee, A., Nguyen-Thoi, T., Li, Z., 2019. Solidification inside a clean energy storage unit utilizing phase change material with copper oxide nanoparticles. *J. Cleaner Prod.*, 118888. <https://doi.org/10.1016/j.jclepro.2019.118888>.
- Wang, X., Sun, X., Lao, J., He, H., Cheng, T., Wang, M., Wang, S., Huang, F., 2014. Multifunctional graphene quantum dots for simultaneous targeted cellular imaging and drug delivery. *Colloids Surf. B* 122, 638. <https://doi.org/10.1016/j.colsurfb.2014.07.043>.
- Yang, Y., Xiao, X., Xing, X., Wang, Z., Zou, T., Wang, Z., Zhao, R., Wang, Y., 2019. One-pot synthesis of N-doped graphene quantum dots as highly sensitive fluorescent sensor for detection of mercury ions water solutions. *Mater. Res. Express* 6, 095615. <https://doi.org/10.1088/2053-1591/ab3006>.
- Ding, Y., Wang, S., Li, J., Chen, L., 2016. Nanomaterial-based optical sensors for mercury ions. *TrAC, Trends Anal. Chem.* 82, 175. <https://doi.org/10.1016/j.trac.2016.05.015>.
- Dong, Y., Shao, J., Chen, C., Li, H., Wang, R., Chi, Y., Lin, X., Chen, G., 2012. Blue luminescent graphene quantum dots and graphene oxide prepared by tuning the carbonization degree of citric acid. *Carbon* 50, 4738. <https://doi.org/10.1016/j.carbon.2012.06.002>.

- Wang, Y., Hu, A., 2014. Carbon quantum dots: synthesis, properties and applications. *J. Mater. Chem. C* 2, 6921. <https://doi.org/10.1039/C4TC00988F>.
- Zhang, Y., Cui, P., Zhang, F., Feng, X., Wang, Y., Yang, Y., Liu, X., 2016b. Fluorescence probes for “off-on” highly sensitive detection of Hg²⁺ and L-cysteine based on nitrogen-doped carbon dots. *Talanta* 152, 288.
- Li, Z., Wang, Y., Ni, Y., Kokot, S., 2015. A rapid and label-free dual detection of Hg (II) and cysteine with the use of fluorescence switching of graphene quantum dots. *Sens. Actuators, B* 207, 490. <https://doi.org/10.1016/j.snb.2014.10.071>.
- Liu, Z., Gong, Y., Fan, Z., 2016. Cysteine detection using a high-fluorescence sensor based on a nitrogen-doped graphene quantum dot–mercury(II) system. *J. Lumin.* 175, 129. <https://doi.org/10.1016/j.jlumin.2016.01.036>.
- Wang, Z., Fan, Z., 2018. Cu²⁺ modulated nitrogen-doped grapheme quantum dots as a turn-off/on fluorescence sensor for the selective detection of histidine in biological fluid. *Spectrochim. Acta Part A Mol. Biomol. Spectrosc.* 189, 195.
- Xue, Z., Gao, X., Li, X., 2018. A Green and lower-temperature synthesis of two-color fluorescent nitrogen doped graphene quantum dots. *Dyes. Pigments.* 156, 379. <https://doi.org/10.1016/j.dyepig.2018.04.032>.
- Yan, Z., Qu, X., Niu, Q., Tian, C., Fan, C., Ye, B., 2016. A green synthesis of highly fluorescent nitrogen-doped graphene quantum dots for the highly sensitive and selective detection of mercury(II) ions and biothiols. *Anal. Methods* 8, 1565. <https://doi.org/10.1039/C5AY03208C>.